Mode Conversion at Discontinuities in Finite-Width Conductor-Backed Coplanar Waveguide

ROBERT W. JACKSON, SENIOR MEMBER, IEEE

Abstract—**The effect of overmoding in a conductor-backed coplanar waveguide is discussed, with special emphasis on mode conversion at discontinuities. The coplanar waveguide gap end and shorted end are studied via a fully electromagnetic application of the moment method technique. Significant conversion occurs at the gap end. The results of a simple experiment are described.**

I. Introduction

COPLANAR WAVEGUIDE (CPW) is a circuit medium that is sometimes considered as an alternative to microstrip lines in millimeter-wave integrated circuits. Its principal advantage is the location of the signal grounds on the same substrate surface as the signal line. This eliminates the need for via holes and thus simplifies the fabrication process [1]. It also reduces the parasitic inductance which occurs in grounding field effect transistors. One disadvantage to the CPW is that both an even and an odd mode (with respect to current) can exist. The latter mode is commonly removed by short-circuiting it with air bridges [1].

In practice, additional conducting planes are often present above and below the substrate (see Fig. 1(a)) in order to separate the circuit from its environment. In addition, the lower conducting plane usually contacts the substrate in order to improve heat dissipation. The standard CPW plus the lower conducting plane is commonly called conductor-backed, or grounded coplanar waveguide (GCPW). The moding problem that this conductor backing introduces is the subject of this paper.

The structure shown in Fig. 1(a) supports modes which can be lumped into three groups: (1) the modes (usually one) guided by the CPW slots, (2) parallel-plate modes guided between the CPW plane and the lower conducting plane, and (3) parallel-plate modes guided by the cover. The third group of modes is relatively less important than the first two groups and will not be emphasized in what follows. Of the second group, only the lowest order mode is usually present and it can serve as a vehicle for energy leakage from the CPW. As discussed by Oliner [2] (see also [3]), leakage occurs when the phase velocity of the parasitic mode is slower than the phase velocity of the fundamental mode. It is usually a continuous function of frequency with a leakage angle that varies such that the parasitic mode velocity projected along the fundamental mode direction matches the fundamental mode velocity. In a conductor-backed CPW, the parallel-plate mode is always slower than the fundamental CPW mode and thus leakage occurs.

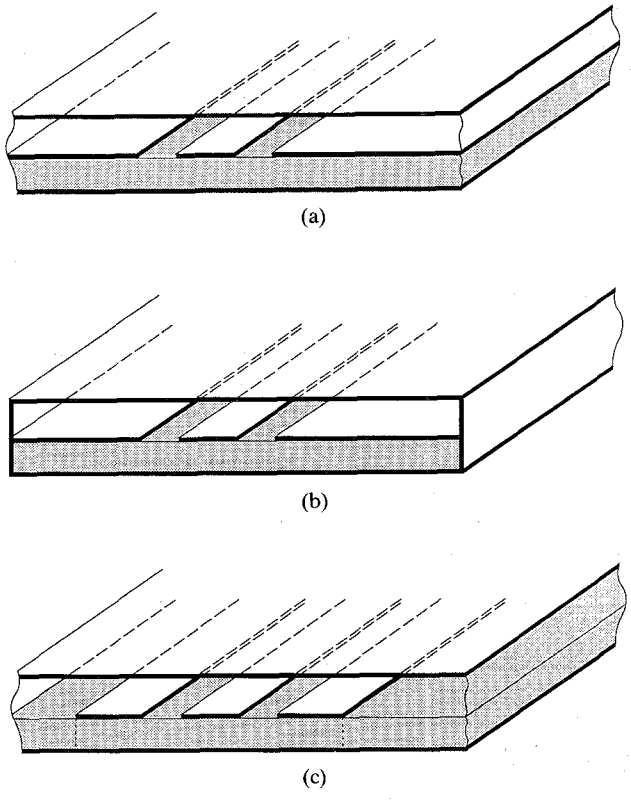

Fig. 1. Conductor-backed coplanar waveguide with (a) infinite lateral extent, (b) shorting sidewalls, and (c) finite-width side planes.

Most practical CPW structures are not of infinite lateral extent, but are limited as in Fig. 1(b) and (c). Mode interactions in these cases are related to the leakage previously discussed, but are very different. In Fig. 1(b), the shaded parallel-plate region is bounded by electric sidewalls. Similarly, the shaded parallel-plate region in Fig. 1(c) is bounded, approximately, by magnetic sidewalls, as indicated by the dashed lines. Because of these boundaries,

Manuscript received February 16, 1989; revised June 1, 1989.
The author is with the Department of Electrical and Computer Engineering, University of Massachusetts, Amherst, MA 01003.
IEEE Log Number 8929905.

0018-9480/89/1000-1582$01.00 ©1989 IEEE

the aforementioned parallel-plate wave now becomes a waveguide mode (in Fig. 1(b)) or a microstrip-like mode (in Fig. 1(c)), and qualitatively results from the reflection of the parallel-plate wave at the sidewall boundaries. Interactions between these modes and the CPW mode occur when their longitudinal phase velocities match. In this way they are the same as the leaky wave case. The interactions are different in that they occur only at discrete frequencies and are much stronger. This has been discussed by Shigesawa *et al.* [4]. Such interactions (mode degeneracies) must be avoided since the CPW no longer confines the propagating energy at those frequencies.

Often these interactions can be eliminated over a limited frequency range. In Fig. 1(b), the conducting sidewalls may be moved in close enough that the parasitic mode is cut off entirely. At high frequencies, with high-permittivity substrates, this becomes very difficult to do. For example, if the substrate in Fig. 1(b) has a dielectric constant of 13 (GaAs) and an operating frequency of 40 GHz, the lateral dimension of the substrate must be less than 1 mm in order to cut off the waveguide mode. If the structure is operated above cutoff, the wall separation may be adjusted so as to preclude a phase match between the waveguide and CPW modes within a specified frequency range. However, this is difficult or impossible to do over a wide band of frequencies.

The structure in Fig. 1(c) has been used for tape automated bonding (TAB) applications [5]. As stated previously, it can be thought of as having magnetic walls lying along the dashed lines in the figure. The disadvantage of this structure is that the lowest order waveguide mode (microstrip-like) has a zero frequency cutoff and thus cannot be eliminated. For high-frequency, wide-band operation it has two advantages over the structure in Fig. 1(b). Since the lateral extent of the guiding structure is determined by the side plane conductors and not the substrate, it can be made as small as necessary in order to eliminate higher order waveguide modes. In addition, the lowest order waveguide mode (which cannot be eliminated) always has a slower phase velocity than the CPW mode, and thus a phase match cannot occur. Therefore, the infinitely long CPW in Fig. 1(c) is apparently preferable to the CPW in Fig. 1(b) for wide-band applications.

Since the configuration in Fig. 1(c) is always overmoded, it suffers the same problems that an overmoded rectangular waveguide suffers. At discontinuities, energy couples from one mode to the other. Reference [6] studies the coupling between modes at discontinuities by studying the characteristics of these modes on an infinite line. As will be seen, the amount of coupling depends on the details of a particular discontinuity and not only on the infinite line characteristics. In this paper, this coupling is very accurately calculated for the gap-end and shorted-end discontinuities. Fig. 2 shows the specific configuration which is analyzed. Setting the thickness of substrate 1 in the figure to zero results in a conductor-backed CPW input line. An approximation to an ideal open circuit is created when the gap is made large enough that further changes in gap size have little effect on the end impedance of the line. Reducing the gap to zero creates an approximation to the ideal short circuit. For lack of a better term, this will be called a CPW shorted end.

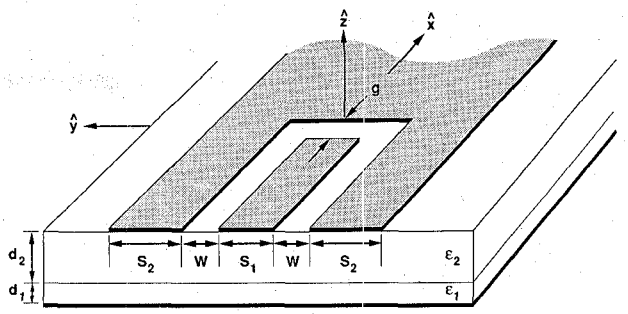

Fig. 2. Configuration of the CPW gap-end ($g \neq 0$) or shorted-end ($g = 0$) discontinuity.

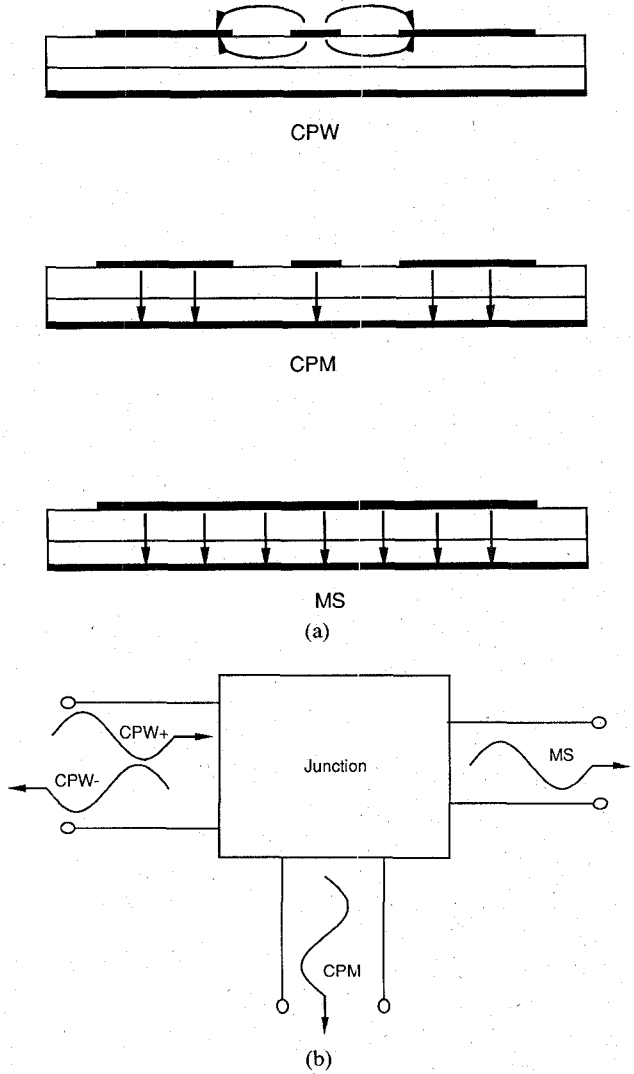

Fig. 3. (a) Schematic model of the field lines for the three modes of interest. (b) Three port model of the CPW discontinuity.

There are three modes which are significant in this setup. They are illustrated schematically in Fig. 3. In the transmission line leading up to the gap, only the first two modes shown in Fig. 3 can propagate and they are desig-

nated CPW (coplanar waveguide) and CPM (coplanar microstrip). Only the third mode in Fig. 3, designated MS (microstrip), propagates beyond the gap to $x = +\infty$. Transverse symmetry is assumed and so no antisymmetric mode is excited. Fig. 3(b) shows schematically the three-port formed by Fig. 2. Ideally, a CPW mode incident on an open or on a short is totally reflected into the same CPW mode propagating in the reverse direction. Here, part of the incident CPW wave is reflected back as a CPW wave, part is reflected back as a CPM wave traveling on the same line, and part is transmitted beyond the discontinuity as an MS mode.

This conversion is important since the CPM or MS modes will not couple to active devices on the CPW surface. It may result in resonances and power suck-outs which could render a circuit inoperable. It should be emphasized that this conversion occurs even if the CPW and CPM modes do not couple on the corresponding infinite line.

In this paper, the simple discontinuity in Fig. 2 is used to determine the degree of coupling which *could* occur and the effect of the configuration on this coupling. It is not an exhaustive treatment of every type of configuration or discontinuity. Some preliminary work was reported in [7], but the configuration presented here is more generic. Related earlier work for radiation on CPW with infinitely wide side planes can be found in [8]. The moment method analysis which is used is fully electromagnetic and is described in the following section. The third section presents numerical results. This is followed by a short description of a simple experiment. Finally, the implications of this work are discussed.

II. Outline of the Analysis

The structure in Fig. 2 is analyzed using a finite element technique which is rigorous in the moment method sense. In other words, the formulation is exact up to the application of the moment method technique. All parallel-plate modes, surface waves, and radiated energies that are present for a particular configuration are included in the integral equation which follows. The procedure is similar to those described in [9], [10], [11], and, especially, [12]. It makes use of a Green's function that relates the surface current on the $z = 0$ surface to the tangential electric field on the same surface. This relationship is expressed in a spectral form as

$$\vec{E}(x, y) = \frac{1}{(2\pi)^2} \iint_{-\infty}^{\infty} \vec{\bar{Q}}(k_x, k_y) \cdot \vec{J}(k_x, k_y) e^{jk_x x} e^{jk_y y}\, dk_x\, dk_y \quad (1)$$

where $\vec{E}(x, y)$ is the two-component surface field, $\vec{J}(k_x, k_y)$ is the Fourier transform of the surface current, and $\vec{\bar{Q}}(k_x, k_y)$ is the Fourier transform of the Green's function. Included in this function is the influence of the two substrates, the conductor backing, and a cover plate above the $z = 0$ surface. This last plate is not shown in Figs. 2 or 3, and is located far enough above the $z = 0$ plane that it has minimal effect on the results presented later. The integrand in (1) has, in general, a number of poles which correspond to parallel-plate waves guided between the cover plate and the conductor backing. These are not the same as the modes in Fig. 3(a), which exist due to the conductor on the $z = 0$ plane. The separation between the conductor backing and the cover is kept small enough that only one parallel-plate mode can be excited and the amount of energy lost to this wave is extremely small. It can be considered as a negligibly small loss within the three-port shown in Fig. 3(b). The function $Q(k_x, k_y)$ is complicated and, to save space, will not be listed here. The reader is referred to [13]. By setting $\vec{E}(x, y)$ in (1) to zero on all the $z = 0$ conductors in Fig. 2, an integral equation for $\vec{J}(x, y)$ is formed. This equation is exact.

The moment method technique is then applied by very accurately approximating $\vec{J}$ with the following expansion:

$$\vec{J} = \sum_{j=1}^{NM} A_j \vec{J}_j^{\,\mathrm{fe}} + R_{\mathrm{CPW}} \vec{J}^{\mathrm{CPW}-} + R_{\mathrm{CPM}} \vec{J}^{\mathrm{CPM}} + T_{\mathrm{MS}} \vec{J}^{\mathrm{MS}} + \vec{J}^{\mathrm{CPW}+} \quad (2)$$

where $\vec{J}^{\mathrm{CPW}-}$, $\vec{J}^{\mathrm{CPM}}$, $\vec{J}^{\mathrm{MS}}$, and $\vec{J}^{\mathrm{CPW}+}$ are precomputed currents which are predominantly sinusoidal and which have known forms (propagation constants, x and y dependence, x and y vector components). They correspond to the reflected CPW wave, the reflected CPM wave, the transmitted MS wave, and the incident CPW wave, respectively. The $\vec{J}_j^{\,\mathrm{fe}}$ are finite element rooftop currents, some of which are x-directed and some y-directed. NM is the total number of finite element currents. A_j, R_{CPW}, R_{CPM}, and T_{MS} are complex coefficients that are determined via the moment method procedure. This procedure is invoked by taking weighted averages of the electric field in (1) and setting them to zero on the $z = 0$ conductor surface according to

$$-\iint_{-\infty}^{\infty} \vec{W}_i(x, y) \cdot \vec{E}(x, y)\, dx\, dy = 0, \qquad i = 1, 2, 3, \cdots, NM + 3 \quad (3)$$

where $\vec{W}_i$ are the weighting functions. The first NM weighting functions are the same as the finite element expansion functions. The last three are described later. The matrix equation which results from combining (1), (2), and (3) has the form

$$\left[\vec{\bar{Z}}\right] \cdot \begin{bmatrix} \vdots \\ A_j \\ \vdots \\ R_{\mathrm{CPW}} \\ R_{\mathrm{CPM}} \\ T_{\mathrm{MS}} \end{bmatrix} = -\left[\vec{Z}^{+}\right] \quad (4)$$

where the $\vec{\bar{Z}}$ matrix results from testing the first four types of expansion functions in (2), and the vector $\vec{Z}^{+}$ results

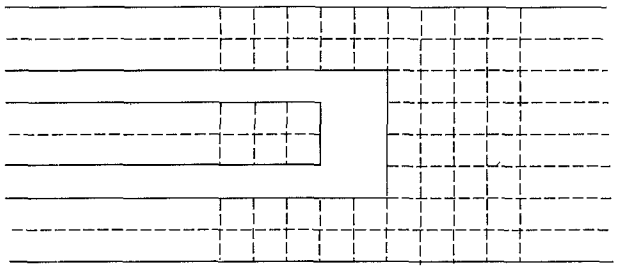

Fig. 4. The grid used in the finite element analysis of the discontinuities.

from testing the incident current $\vec{J}^{\mathrm{CPW}+}$. A typical member of $\vec{\vec{Z}}$ has the form

$$Z_{i\,\mathrm{MS}} = \frac{1}{(2\pi)^2}\iint_{-\infty}^{\infty} dk_x\,dk_y\left[J_{iy}^{fe}(k_x,k_y)\right]^* \cdot Q_{yx}(k_x,k_y)J_x^{\mathrm{MS}}(k_x,k_y). \quad (5)$$

Impedances such as this are carefully evaluated in order to take into account the poles of Q arising from the (cover plate, conductor backing) parallel-plate modes mentioned previously.

Rooftop functions are used for expansion and weighting in the discontinuity area. These functions are arranged in a grid similar to Fig. 4. When the shorted end is modeled by reducing g to zero, additional rooftop functions are added in order to ensure current continuity across the $x = 0$ line. Both x- and y-directed functions are used. All x-directed rooftop functions are of the same size. The same is true for all y-directed rooftop functions. This vastly speeds the analysis. Further detail can be found in [12].

The incident, reflected, and transmitted waves are all precomputed and have the form

$$\vec{J}^{\mathrm{CPW}\mp} = \left[g_x^{\mathrm{CPW}}(y)\hat{x} \mp jg_y^{\mathrm{CPW}}(y)\hat{y}\right] \cdot\left[\cos(\beta^{\mathrm{CPW}}x) \pm j\sin(\beta^{\mathrm{CPW}}x)\right] \quad (6a)$$

$$\vec{J}^{\mathrm{CPM}} = \left[g_x^{\mathrm{CPM}}(y)\hat{x} - jg_y^{\mathrm{CPM}}(y)\hat{y}\right] \cdot\left[\cos(\beta^{\mathrm{CPM}}x) + j\sin(\beta^{\mathrm{CPM}}x)\right] \quad (6b)$$

$$\vec{J}^{\mathrm{MS}} = \left[g_x^{\mathrm{MS}}(y)\hat{x} + jg_y^{\mathrm{MS}}(y)\hat{y}\right] \cdot\left[\cos(\beta^{\mathrm{MS}}x) - j\sin(\beta^{\mathrm{MS}}x)\right] \quad (6c)$$

where the propagation constants β^{CPW}, β^{CPM}, β^{MS} and the functions g_x^{CPW}, g_y^{CPW}, g_x^{CPM}, g_y^{CPM}, g_x^{MS}, and g_y^{MS} are computed from a full-wave analysis of the infinite line. Pulse functions are used in modeling g_x (see Fig. 5), and triangular functions are used in modeling g_y (not shown). The sizes of these pulse and triangular functions are commensurate with the rooftop functions used in the junction area. In the discontinuity calculation, the sinusoidal x dependence of (6) is truncated in a manner similar to the truncation described in [12]. The $g_x(y)$ functions are also combined with a triangular x dependence and used as the last three weighting functions mentioned previously (see also [12]).

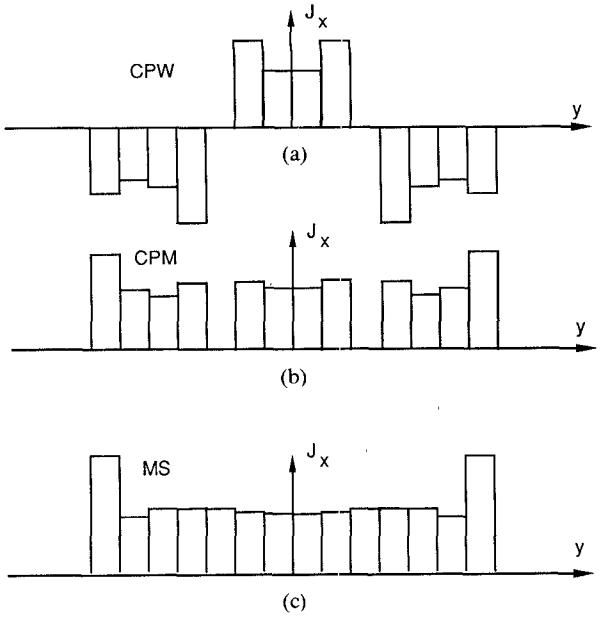

Fig. 5. Pulse function approximation of the current densities associated with each mode.

Once the coefficients R_{CPW}, R_{CPM}, and T_{MS} are determined by solving (4), they are used to determine the power flowing in each mode by integrating the Poynting vector over the cross section of the various lines. This is simple in principle, but involves some tedious algebra. As an intermediate step, the impedances of each line are calculated according to the power–current definition of impedance where the currents in these definitions are, for the CPW and CPM modes, the total current on the center strip ($|y| < S_1/2$) and, for the MS mode, the overall strip current ($|y| < S_1/2 + W + S_2$). R_{CPW} and R_{CPM} are then used to calculate the center strip currents of the reflected waves. T_{MS} is used to calculate the total strip current of the transmitted wave. These are then combined with the aforementioned impedances to calculate the various reflected and transmitted powers.

III. Numerical Results

The results which follow have been checked via several methods. Those shown in Figs. 6, 7, and 8 have been computed using approximately 15 columns of elements (see Fig. 4) distributed in the range $|x| < 3d_2$. For Figs. 6 and 7, 16 to 24 rows of elements were used. This totals to roughly 250 to 350 x-directed elements and not quite that many y-directed elements. Symmetry reduces the size of the computation by a factor of 2, and a number of additional techniques have been used to speed the process. By varying the number and the spacing of these elements, the calculated values of R_{CPW}, R_{CPM}, and T_{MS} are estimated to be within 3 percent of full convergence. The results shown in Fig. 8 are computed using half the number of rows mentioned above, but the same number of columns. In that case the convergence is estimated to be better than 6 percent. This is far more accuracy than is necessary for this application.

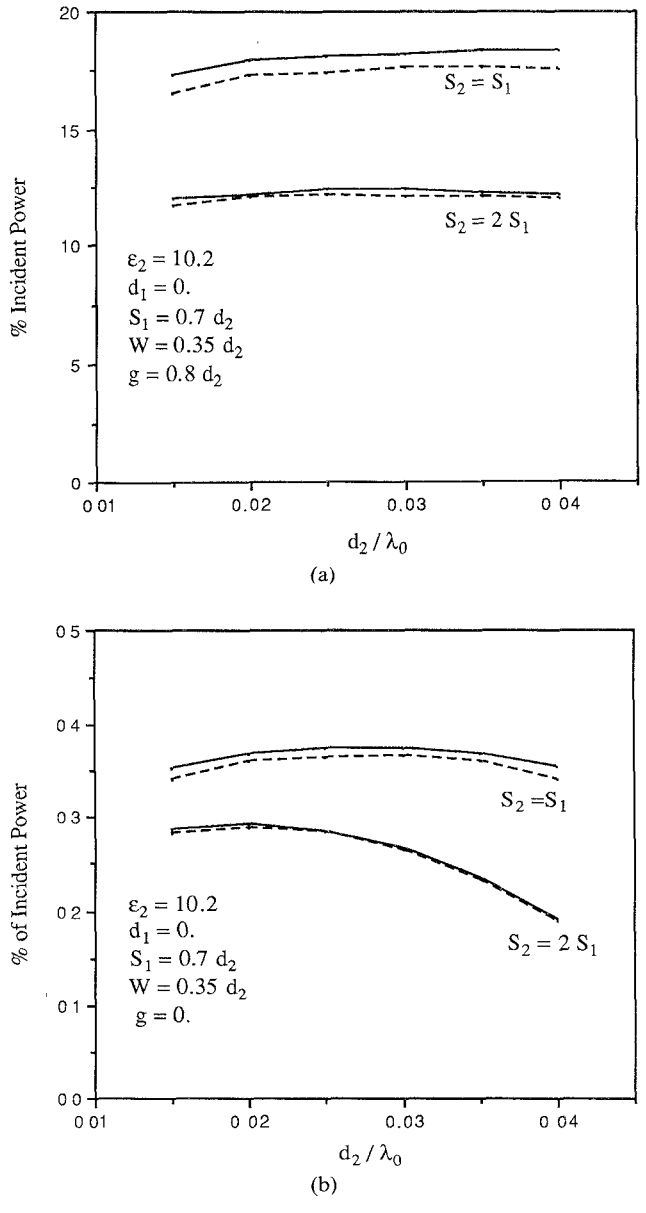

Fig. 6. Percentage of incident CPW power converted to the transmitted MS mode (———) and the reflected CPM mode (– – – –) versus normalized frequency for (a) a gap end and (b) a shorted end.

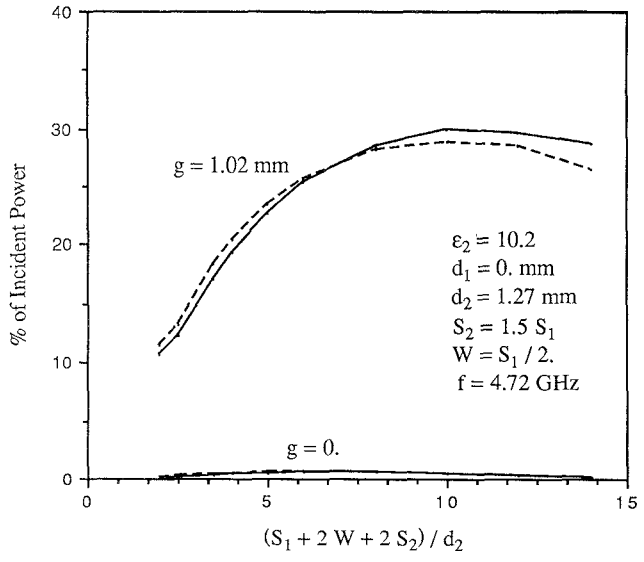

Fig. 7. Percentage of incident CPW power converted to the transmitted MS mode (———) and the reflected CPM mode (– – – –) versus CPW size.

Each point calculated in Fig. 8 used about 20 minutes on a MICROVAX computer. There are a number of numerical techniques which could be applied to the analysis in order to greatly reduce this time. For this particular application, the added complexity was not worth the time savings.

A few other details should be mentioned. The structures which are considered have CPW impedances of roughly 50 Ω, and thus the slots are not so narrow that the slot edges are very tightly coupled. The set of expansion functions described above does include coupling between the slots and is capable of accurate results even with reasonably tight coupling. If, however, a structure with very tight coupling (as in a Lange coupler) were to be analyzed with a high degree of accuracy, a set of expansion functions that do a better job of modeling the edge currents might be necessary. The phase angles of R_{CPW} were roughly correct, being slightly capacitive when a fairly wide gap is present and slightly inductive when a shorted end is calculated. The sum of the reflected CPW, reflected CPM, and transmitted MS powers was equal to the incident power within a small fraction of the coupled power. A negligible fraction of the incident power is transferred to the parallel-plate wave which exists between the cover and the conductor backing.

Fig. 6 shows the percentage of incident power that is converted into a transmitted MS mode and also the percentage that is converted into a reflected CPM mode. These are plotted versus normalized frequency for two side plane sizes. For an approximate CPW open ($g = 0.8$ substrate thicknesses), Fig. 6(a) shows that when $S_2 = 2S_1$, roughly 12 percent of the incident CPW power is converted to a transmitted microstrip mode and an equal amount converts to a reflected CPM mode. Only about 75 percent of the incident CPW power is reflected back as a CPW mode and this fraction is relatively constant with respect to frequency. Fig. 6(b) shows that changing the discontinuity from an approximate open circuit to a shorted end ($g \rightarrow 0$) decreases converted power by a factor of almost 50. In both cases, the power converted to the MS mode is nearly the same as the power converted to the CPM mode. This is not surprising in view of the similar field configurations of the two modes (see Fig. 3) and their very similar propagation constants.

Fig. 7 shows the effect of increasing the size of the CPW with respect to substrate thickness for a fixed frequency. Smaller structures convert less power and, once again, the power converted at a shorted end is much less than at a gap end.

Fig. 8(a) shows some interesting effects that result from the addition of a low-permittivity layer between the substrate and the conductor backing. Referring to Fig. 2, all

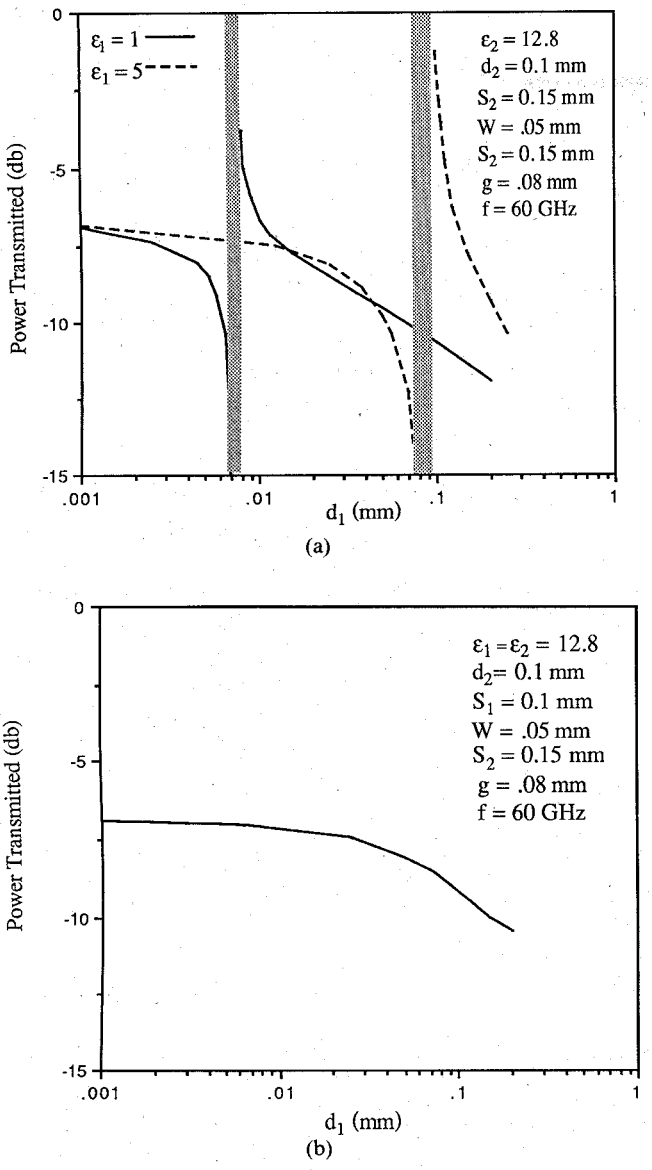

Fig. 8. Conversion (in dB) of the incident CPW mode to the transmitted MS mode at a gap end versus the thickness of an additional substrate with dielectric constants of (a) $\epsilon_1 = 1.0$ (———) and $\epsilon_1 = 5.0$ (– – – –) and (b) $\epsilon_1 = 12.8$.

parameters are held constant except the thickness of dielectric 1. Fig. 8(a) plots transmitted power versus slab 1 thickness for two different slab 1 dielectrics. For each dielectric, the fraction of incident power converted to the MS mode (in dB) gradually decreases as the thickness increases until a specific thickness is reached. As substrate 1 approaches this thickness, a sharp drop in converted power is observed. For thicknesses just larger than this value, the converted power is very large and then decreases. The power reflected into the CPM mode behaves almost exactly the same way except for thicknesses very near this singular thickness and there the response of the two modes is still qualitatively the same. This special thickness corresponds to the value of d_1 which results in the effective dielectric constants of the CPW, CPM, and MS modes being equal. The effective dielectric constant of the CPW mode is relatively insensitive to d_1 and can be estimated by

$$\epsilon_{e,\mathrm{CPW}} \sim (\epsilon_2 + 1)/2. \tag{7}$$

The effective dielectric constants of the CPM and MS modes are roughly equal to each other and are both sensitive to d_1. They can roughly be determined by

$$\epsilon_{e,\mathrm{CPM}} \simeq \epsilon_{e,\mathrm{MS}} \sim (d_1 + d_2) \Big/ \left(\frac{d_1}{\epsilon_1} + \frac{d_2}{\epsilon_2} \right). \tag{8}$$

The singular value of d_1 can be estimated by equating (7) and (8) such that

$$\bar{d}_1 \sim \frac{d_2(\epsilon_2 - 1)\epsilon_1}{(\epsilon_2 + 1 - 2\epsilon_1)\epsilon_2}. \tag{9}$$

Near this value, the CPW and CPM modes on the input line are nearly degenerate, as discussed in [4] and in the introduction. For values of d_1 in the shaded region of Fig. 8(a), this near degeneracy caused the determination of the precomputed currents in (6) to become unreliable. Changing the gap end to a shorted end ($g = 0$) results in a conversion curve having roughly the same shape but reduced by about 15 dB.

For comparison, Fig. 8(b) shows how the conversion varies with substrate thickness if substrate 1 has the same dielectric constant as substrate 2. In this case, the effective dielectric constant of the CPM and MS modes always remains greater than that of the CPW mode. Thus, no degeneracy will occur and the peaking seen in Fig. 8(a) will not occur.

In the case where $\epsilon_1 = 5.0$ or 12.8, care has been taken to ensure that the cover plate (as in Fig. 1(c)) is not so far above the conductor backing that a TE_z mode is allowed to propagate between them. Only the lowest TM_z mode is allowed to propagate in the examples discussed herein and the energy lost to it is relatively insignificant. Also, none of the structures have been made wide enough to allow a higher order CPM or MS mode.

IV. Experiment

In addition to the numerical results presented in Figs. 6, 7, and 8, a couple of simple measurements were made which partially verify the analysis. The discontinuity shown in Fig. 2 was constructed on a 1.27-mm-thick Duroid substrate ($d_1 = 0$) with a relative permittivity of 10.2. The dimensions of the structure were $S_1 = S_2 = 0.90$ mm and $W = 0.64$ mm. The incident mode is launched via an SMA connector on the CPW line with no conductor backing; conductor backing was then gradually tapered in up to the discontinuity. Beyond the discontinuity, the microstrip line on the top surface was tapered down to an impedance of 50 Ω and fed to another SMA connector. The entire assembly was about 16 cm long. The transmission response of the network was measured versus frequency from 2 to 15 GHz using an HP 8510 network analyzer. The 8510 gating option allowed removal of the extraneous transmission pulses which occur due to secondary reflections. The

resulting frequency response after gating showed the transmission response of the connectors, tapers, and discontinuity. For a shorted-end discontinuity, the transmission measurement was unreliable since it was very small and difficult to distinguish from energy launched at the taper which precedes it. All that can be said is that the conversion was less than -20 dB. When a gap of about 0.9 mm was cut, the transmission increased to about -8.7 dB ± 0.6 across the frequency range of interest (3.4–9.5 GHz). The results in Fig. 6 for a similar configuration show a transmission of about -7.5 dB. This is reasonably close to the measured transmission if one includes connector loss and taper mismatch.

V. Discussion

Only two discontinuities have been studied in this work. However, these indicate several important points. Obviously, a planar line which is overmoded has the same problems that an overmoded rectangular waveguide has—mode conversion at discontinuities. Just because a *uniform* transmission line is designed not to leak energy (infinite lateral extent) or not to couple to extra modes (finite lateral extent) does not preclude the possibility that coupling will occur when a nonuniformity is introduced. As evidenced by Fig. 6, the coupling can be very severe (the gap end), or not very severe at all (the shorted end), depending on the discontinuity. This coupling can cause resonances and suck-outs for high frequency circuits or ringing in the case of a digital circuit. The ease with which one can in practice minimize these effects (by adding lossy layers, for example) depends upon the degree of coupling.

Fig. 8 shows that a dielectric layer between the conductor backing and the substrate can have a very pronounced effect. A few microns of air gap beneath a high-permittivity substrate can result in widely varying coupling. A gap of a few hundred microns reduces the conversion significantly. An air gap may not be possible if heat sinking for active devices is a concern. In that case, a layer of low-permittivity dielectric with good thermal conductivity (diamond, for example) may be useful. Fig. 8(a) shows that a 50–60 μm thick layer with a dielectric constant of 5 may reduce the conversion. A much thicker layer, several hundred microns thick, would also work. However, there is a possibility that a very thick layer would turn on a TE_z mode guided between the cover plate and the conductor backing. Fig. 8(b) shows that just thickening the high-dielectric substrate will also reduce the conversion, although it may need to be fairly thick for a substantial reduction. A silicon ($\epsilon = 12$) substrate under a GaAs substrate would have the same effect. Fig. 7 actually shows this effect in a different way. It shows that the coupling can be reduced if the size of the structure, relative to the dielectric thickness, is reduced.

In summary, if no air gap is possible due to heat dissipation requirements, a thick substrate and a small guide cross section ($S_1 + 2W$) should reduce conversion. Discontinuities similar to the gap end are particularly good converters and should be avoided. Note also, this assumes that via holes between the side conductors of the CPW and the conductor backing are not desirable. Vias would, of course, short-circuit the CPM and MS modes.

Some of the results presented here can be approximately applied to the shorted sidewall configuration shown in Fig. 1(b). Since the sides of Fig. 1(c) can be considered as roughly open circuits, replacing them by quarter-wavelength side plane extensions that are terminated in a short circuit should not change the circuit behavior. Thus, in Figs. 6, 7, and 8(b), the overall width of the equivalent shorted sidewall guide would be

$$W_{\text{total}} = S_1 + 2W_1 + 2S_2 + \lambda_0/\sqrt{\epsilon_2}/2 \qquad (10)$$

and the amount of energy converted from an incident CPW mode to a waveguide mode could be estimated. This type of estimation is most accurate when $S_2/(d_2 + d_1)$ is much greater than 1.

Finally, note that discontinuities that are not planar may also launch microstrip-like modes. Specifically coaxial connectors, which launch a CPW mode, may also launch these parasitic CPM waves.

VI. Conclusions

Mode conversion at two types of discontinuity has been investigated numerically for a version of conductor-backed coplanar waveguide. Substantial conversion can occur depending on the type of discontinuity. The effects of the underlying substrate configuration on this phenomenon were studied.

References

[1] M. Riaziat *et al.*, "Coplanar waveguide used in a 2–18 GHz distributed amplifier," in *IEEE MTT-S Int. Microwave Symp. Dig.*, 1986, pp. 337–338.

[2] A. A. Oliner and K. S. Lee, "The nature of the leakage from higher order modes on microstrip line," in *IEEE MTT-S Int. Microwave Symp. Dig.*, 1986, pp. 57–60.

[3] D. P. Kasilingam and D. B. Rutledge, "Surface-wave losses of coplanar transmission lines," in *IEEE MTT-S Int. Microwave Symp. Dig.*, 1983, pp. 113–116.

[4] H. Shigesawa, M. Tsuji, and A. A. Oliner, "Conductor-backed slot-line and coplanar waveguide: Dangers and full wave analyses," in *IEEE MTT-S Int. Microwave Symp. Dig.*, 1988, pp. 199–202.

[5] S. M. Wentworth, D. P. Neikirk, and C. R. Brahce, "High frequency characterization of tape-automated bending (TAB) interconnects," in *SPIE Proc. Interconnection of High Speed and High Frequency Devices and Syst.*, vol. 947, pp. 81–84, Mar. 1988.

[6] M. Riaziat *et al.*, "Single-mode operation of coplanar waveguides," *Electron. Lett.*, vol. 23, Nov. 19, 1987.

[7] R. W. Jackson, "Mode conversion at discontinuities in modified grounded coplanar waveguide," in *IEEE MTT-S Int. Microwave Symp. Dig.* (New York), 1988, pp. 203–206.

[8] R. W. Jackson, "Considerations in the use of coplanar waveguide for millimeter wave integrated circuits," *IEEE Trans. Microwave Theory Tech.*, vol. MTT-34, pp. 1450–1456, 1986.

[9] R. H. Jansen, "High-order finite element polynomials in the computer analysis of arbitrarily shaped resonators," *Arch. Elek. Übertragung.*, vol. 30, pp. 71–79, 1976.

[10] J. R. Mosig and F. E. Gardiol, "General integral equation formulation for microstrip antennas and scatterers," *Proc. Inst. Elec. Eng.*, vol. 132, pt. H, no. 7, pp. 424–432, 1985.

[11] J. C. Rautio and R. F. Harrington, "An electromagnetic time-harmonic analysis of shielded microstrip circuits," *IEEE Trans. Microwave Theory Tech.*, vol. MTT-35, pp. 726–730, 1987.

[12] Jackson, R. W., "Full-wave finite element analysis of irregular microstrip discontinuities," *IEEE Trans. Microwave Theory Tech.*, vol. 37, pp. 81–89, Jan. 1989.

[13] J. J. Burke and R. W. Jackson, "Surface-to-surface transition via electromagnetic coupling of microstrip and coplanar waveguide," *IEEE Trans. Microwave Theory Tech.*, vol. 37, pp. 519–525, Mar. 1989.

✠

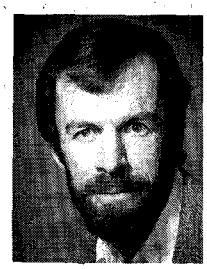

Robert W. Jackson (M'82–SM'88) was born in Boston, MA, in 1952. He received the B.S. (1975), M.S. (1979), and Ph.D. (1981) degrees in electrical engineering from Northeastern University, in Boston. His dissertation was concerned with nonlinear plasma interactions in the bow shock of the earth.

From 1981 to 1982, he was an Assistant Professor in the Department of Electrical Engineering at Northeastern University. Since 1982, he has been on the faculty of the Department of Electrical and Computer Engineering at the University of Massachusetts at Amherst, where he is currently an Associate Professor. His research interests include the electromagnetic aspects of integrated circuits, novel printed circuit and antenna structures, modeling and design of planar ferrite devices, electromagnetics applied to nonlinear or anisotropic materials, and active microwave circuit design.